BIOPHYSICAL
CHEMISTRY

Morphology of DNA–Surfactant Complexes after Their Passing through the Water–Chloroform Interface as Studied by Atomic Force Microscopy

A. S. Andreeva*, M. O. Gallyamov**, O. A. Pyshkina*, V. G. Sergeev*, and I. V. Yaminskii**

*Chemical Faculty, Moscow State University, Vorob'evy gory, Moscow, 119899 Russia
**Center of Modern Technologies, Moscow, Russia
Received October 5, 1998

Abstract—A statistical analysis of AFM images of DNA–surfactant complexes passed into chloroform from the aqueous phase was performed. A universal mathematical model that made it possible to reconstruct the true geometry of objects from their AFM image was developed. This model was used to determine the number of DNA molecules in individual complexes. The histograms of the distribution of complexes over the number of molecules in the complex were constructed, which showed that 80% of the DNA–surfactant complexes contained from 2 to 15 DNA molecules.

INTRODUCTION

It is known that various multivalent cations can cause the condensation of DNA macromolecules in solutions [1]. We demonstrated [2] that the interaction of DNA molecules with cationic surfactants in the aqueous phase is accompanied by the formation of compact complexes with a toroidal morphology. The conclusion about the toroidal structure of the complexes was made on the basis of data obtained by scanning tunnel microscopy (STM).

Since DNA–surfactant complexes are insoluble in water but soluble in organic solvents (chloroform, heptane, cyclohexane) [3], it is interesting to study the process of transfer of DNA–surfactant complexes from the aqueous to the organic phase and to examine the structure of the passed complexes. Such a system can be considered as a model of the process of transmembrane transfer of DNA [4].

The structure of DNA–surfactant complexes was studied by atomic force microscopy (AFM) [5]. AFM makes it possible to obtain images of organic and biological complexes adsorbed at the surface of various supports with a sub-nanometer resolution [6]. In contrast to STM, AFM does no require the use of conducting supports. In addition, AFM images are not affected by the electronic properties of the surface under study; therefore, AFM is more suitable for studying the topographic properties of the object.

In comparison with electron microscopy, AFM has the following advantages. First, there is no limitations on the medium in which the object is examined; second, the procedure of preparation of samples is much simpler (for example, it is unnecessary to prepare replicas). This is especially important in view of the complexity of the system under study, because it is necessary to experimentally select an adequate method of immobilization and dispersion (ideally, without aggregation) of the object on the support.

Knowledge of the geometry of compact complexes is important, for example, in studying the composition of the complex (the number of molecules it contains). The accuracy of determination of the geometry of an organic object by electron microscopy is limited by the accuracy of preparation of replicas, which have a granular structure.

The determination of the geometry of such an object as a DNA–surfactant complex by relative method (XRD analysis, viscosimetry, etc.) is complicated by the following circumstance. The relative methods are based on an analysis of a response obtained not from a single microscopic object but from an ensemble of such objects. This response is used to solve an inverse problem of determination of a parameter characterizing the structure of the microscopic object (by invoking a number of assumptions). If the objects of an ensemble are characterized by a distribution over a selected parameter (its value varies from object to object), the accuracy of solution of the inverse problem is essentially limited by the width of this distribution.

AFM makes it possible to determine a number of structural properties and characteristics of a single nanosized or subnanosized object (including its three-dimensional geometry) under conditions of a rigid fixation of the object on the support. At the same time, the method is not free from artifacts. One of them is a lateral broadening of the object's image due to the fact that the probing tip has a finite radius of curvature. The

drawback is difficult to overcome, because a decrease in the radius of the tip (by using sharper probes) results in an increase in the pressure in the region of contact (at the same force of probing), which, in turn, leads to deformations of the probe and the object, and consequently, to an increase in the lateral dimensions of the contact region and in the radii of curvature of the contacting surfaces [7].

The deformation in the region of contact can be reduced by performing the experiment in a liquid, because, in this case, the contact force can be maintained a low level [8]. However, when experiments are performed in liquids, additional problems may arise, the most important of which is that of fixation of the object on the solid support. The DNA–surfactant complexes we studied could not be fixed at traditional AFM (mica, glass) in a liquid. For this reason, we performed the AFM experiments on the determination of the structure of the DNA–surfactant complexes in air with dry samples. To compare the results obtained and to examine the characteristics of the proposed method we also report the results of an AFM study of separate DNA molecules adsorbed at the mica surface in an aqueous-alcohol medium.

In view of the distorting effects of broadening and contact deformations, it is necessary to use a mathematical analysis to recover the real geometric shape of the object. This analysis should be based on some model assumptions on the geometry of the probe and on the shape of the object. We solved this problem in the general form and used it to quantitatively describe the shape of the DNA–surfactant complexes, in particular to determine the number of DNA molecules in the complex.

EXPERIMENTAL

DNA–surfactant complexes were transferred from an aqueous solution into chloroform. The surfactant was distearyldimethylammonium chloride supplied by the Cogyo Kazei Corporation (Japan). The DNA was extracted from the sperm of salmon (GOSNIIOKhT, Russia); it contained 300–500 pairs of bases.

The process of transfer of DNA–surfactant complexes through the interface was monitored with a Specord M40 UV spectrophotometer (Germany). We found that, after the addition of a 1.5 excess of the surfactant to a two-phase water–chloroform system, practical all DNA molecules migrated to the organic phase [9].

AFM measurements were performed on an Nanoscope-III atomic force microscope (Digital Instruments, USA) in air in the contact-mode regime. The microscope was equipped with a Nanoprobe cantilever (Digital Instruments, USA) with a force constant of 0.06 N/m. The probing needle of the cantilever was fab-

ricated from silicon nitride and had a shape of a pyramid. The firm produces such needles with the curvature radii of the tips in the range of 5–40 nm.

The deposition of the samples onto the support was performed in the following manner. A 3-μl drop of the solution was applied onto a fresh chip of mica and was allowed to remain there for 3–5 min, then the mica surface was washed with twice distilled water, dried in air, and scanned.

RESULTS AND DISCUSSION

Atomic Force Microscopy of DNA–Surfactant Complexes

AFM showed that the aqueous phase after an incomplete transfer contains DNA aggregates in the form of filaments 250–2000 nm in length. The formation of long chains probably might occur due to the intermolecular aggregation of DNA molecules, a feature typical of aqueous solutions. The height and FWHM of these structures measured by AFM were 0.3–0.9 nm and 13–25 nm, respectively.

Figure 1 displays the AFM images of the DNA–surfactant complexes that were transferred from the aqueous phase into chloroform, adsorbed on the mica surface, dried, and then scanned in air. To examine the morphology of the complexes, we statistically processed the AFM images of the toroidal structures. The parameters to be analyzed were the tore diameter D, the diameter of the tore cross section d, the height of the tore-like structure (measured from that surface of the
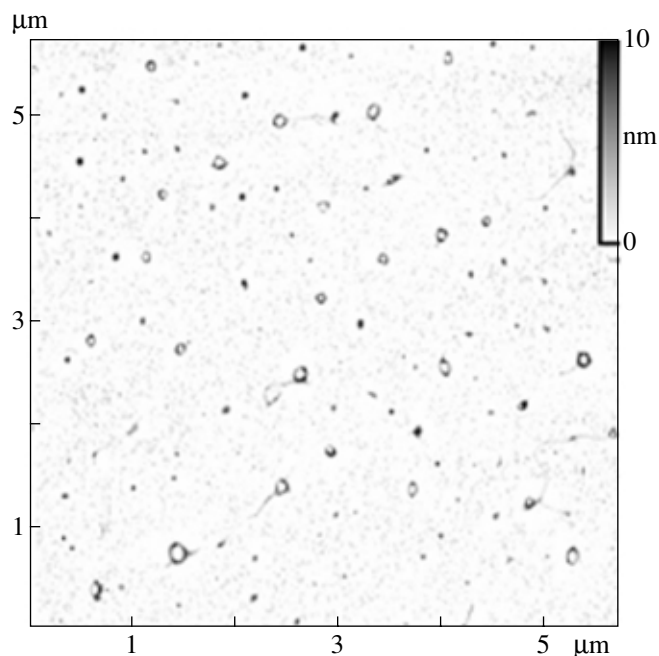

Fig. 1. Toroidal DNA–surfactant complexes that passed into chloroform and were adsorbed at the mica surface (AFM images).
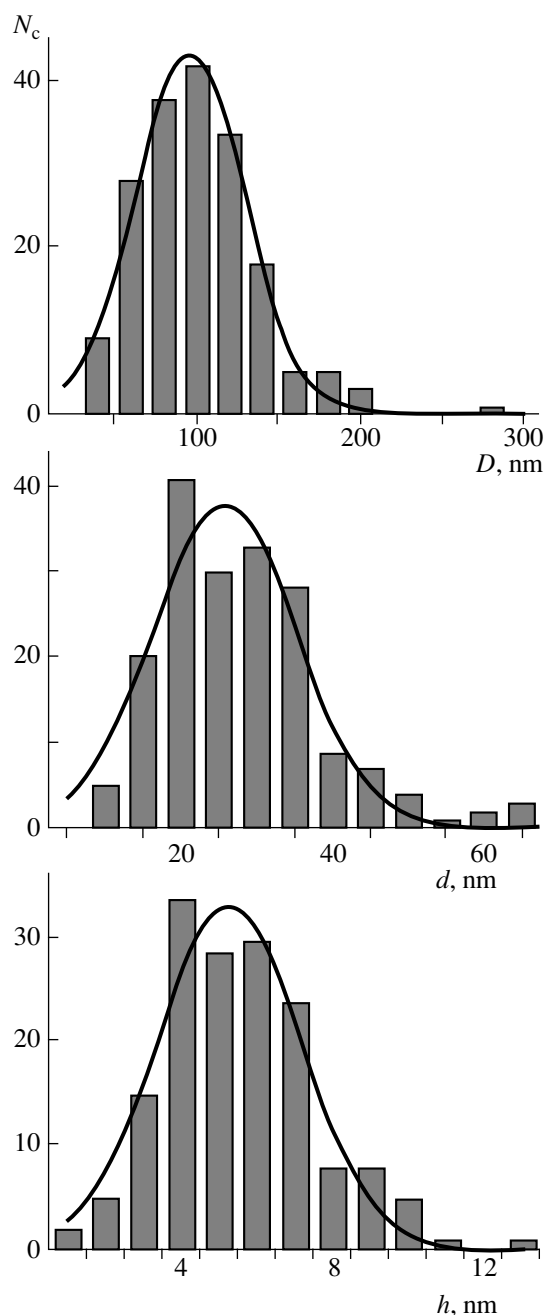
Fig. 2. Histograms of the distribution of toroidal DNA–surfactant complexes over various parameters; D is the tore diameter, d is the diameter of the tore cross section, h is the tore height, and N_c is the number of complexes. The solid line represents the Gaussian approximation.

support) h. The histograms of the distribution of the parameters of the toroidal complexes are displayed in Fig. 2. The solid lines represent the Gaussian approximation of the distributions. These distributions were obtained by processing the shapes of 180 complexes. The averaged parameters of the tore determined from the Gaussian distributions are $D = 100 \pm 30$ nm, $d = 25 \pm 9$ nm, $h = 5 \pm 2$ nm.

Determination of the Number of DNA Molecules in a Complex

Since the length of DNA molecules ranges from 100 to 170 nm, whereas the average length of the circumference πD of the toroidal particles studied was 300 nm, we may conclude that each particle consists of at least 2–3 DNA molecules. A more detailed analysis should involve the reconstruction of the real geometry of the complex.

As mentioned above, AFM is not free from artifacts. For example, the images of individual DNA molecules (according to XRD analysis, the radius of the DNA molecule is about 1 nm) are wider in lateral size (10–15 nm) and lower in height (0.3–1 nm) than the molecule itself [10]. To correct these artifacts, it is necessary to know how they arise.

The height of the object is underestimated because of the deformations caused by the probing needle; this effect is especially significant when the radius of curvature of the object is smaller than that of the needle's tip. This occurs because the surface area of contact in this case is small, and, hence, the pressure produced on the object is high. We assumed that the volume of the object remains constant during measurements; therefore, a decrease in the height ($h = 2b$) is made up by the corresponding increase in the width d. Thus, we postulated that the toroidal complex under study had a flattened shape.

The image is flattened, because the radius of the tip of the probing needle is finite. This effect can be correctly treated on the basis of the known shapes of the tip and the object.

The mechanism of broadening of AFM images is well known for the case when the tip of the needle is parabolic and that of the object is spherical [11]. However, this model is oversimplified, because it does not take into account deformations. A more general model analyzes the contact of the needle with a flattened ellipsoid. Unfortunately, there are no works concerned with applications of this model to real AFM images; this can be explained by a complexity of algebraic expressions involved in such an analysis.

Reconstruction of the Real Geometry of Objects on the Basis of AFM Images

In analyzing the effect of broadening, we used a geometric model (Fig. 3) that takes into account only the interaction of the object with the tip of the needle (there is no contact with the sides of the pyramid). This is justified because the heights of the structures under study do not exceed the radius of the tip. The tip of the probing needle was approximated by either a hemisphere of radius R of by a paraboloid of rotation $y = kx^2$, where k is the coefficient of approximation. It was shown that the results obtained with these two shapes

are virtually the same, the difference is below 3–9%. Since the approximation with a hemisphere is simpler and is more widely used in the literature, we will represent the results obtained with this shape of the tip.

The object was thought of as a flattened tore with diameter D and elliptic cross section semi-axes a and b. The problem was to determine a from the known values of b ($b = h/2$), R (k in this case of the parabolic tip of the needle), and d (d is FWHM of the object).

The elliptic cross-section of the object and the circular cross-section of the tip of the needle are given by

$$\begin{cases} y_e = b(1 - x^2/a^2)^{1/2}, \\ y_c = R - [R^2 - (x - d/2)^2]^{1/2}. \end{cases}$$

For the parabolic shape of the tip, the latter equation takes the form $y_p = k\,(x - d/2)^2$.

The tangents to the ellipse and the circle (parabola) should be equal at the point of contact (x_0, y_0) and the coordinates should satisfy the equations of ellipse and circle:

$$\begin{cases} b(1 - x_0^2/a^2)^{1/2} = R - [R^2 - (x_0 - d/2)^2]^{1/2}, \\ dy_e/dx|_{x_0, y_0} = dy_c/dx|_{x_0, y_0}. \end{cases} \quad (1)$$

For the parabolic shape of the tip, the equation of the parabola should appear in (1).

System (1) was reduced to one equation with one unknown (a), which was solved at various values of R (or k for the parabolic tip of the needle) for each pair of the b ($b = h/2$) and d values from the statistically processed data. It is possible to show analytically that the obtained equation for a spherical tip of the needle has more than one solution if the inequalities

$$\begin{cases} R > d/2, \\ b > R - (R^2 - d^2/4)^{1/2} \end{cases} \quad (2)$$

are satisfied. In this case of a parabolic tip of the needle the inequality $b > kd^2$ should be fulfilled. The meaning of this inequality is obvious: an obtuse needle cannot be used to reproduce a sharp profile. We calculated the percentage of d and b pairs ($b = h/2$) from the accumulated statistics satisfying inequality (2) at various values of R, i.e., the number of cases when system (1) has no solution. Figure 4 shows the number of cases of solution absence versus R. A similar plot was obtained for the parabolic tip of the needle (versus k).

According to special tests (for example, by using the tobacco mosaic virus—a convenient natural nanosized object with well known geometric parameters [12]), the curvature radius of the needle's tip for the cantilevers used ranges from 5 to 20 nm (according to the producer up to 40 nm). For a parabolic tip of the needle, this cor-
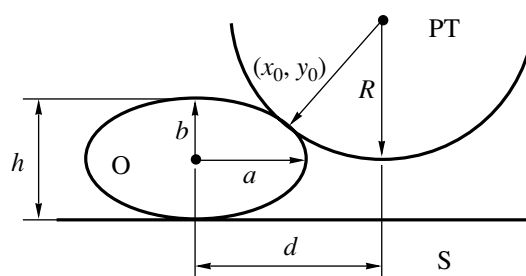

Fig. 3. Illustrating the mechanism of image broadening: PT is the probing tip, O is the object, and S is the support.
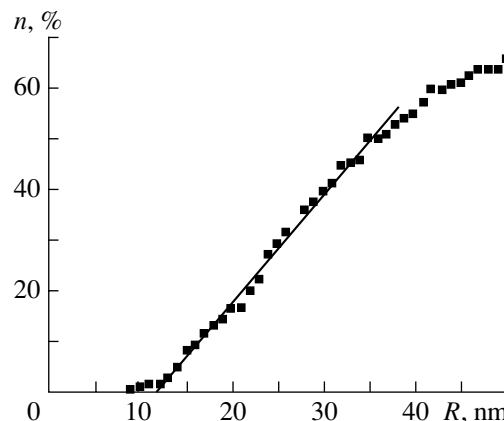

Fig. 4. The fraction (%) of cases of solution absence n for system (1) (for accumulated statistics of the values of d–h pairs) as a function of the radius of curvature of the probing tip R.

responds to $k = (21.5–3.9) \times 10^{-2}$ nm^{-1}. To accurately determine the radius R (or k) for a given needle, it is necessary to test it intermediately before experiments. However, a probability remains that the shape of the tip may be changed during measurements. In this connection, it is extremely important to obtain information on the shape of the probing tip from the AFM image of the object. For example, Fig. 4 makes it possible to conclude that the upper limit of R is 12 nm (or $k = 5.5 \times 10^{-2}$ nm^{-1}). Above these values, a linear growth of the number of cases of solution absence is observed. The lower boundary for the curvature radius of the probing tip is controlled by contact deformations.

We calculated the number of molecules per each toroidal structure using two various values of R (6 and 12 nm, which correspond to $k = 13.2 \times 10^{-2}$ and 5.5×10^{-2} nm^{-1}). The average values of a (determined numerically) for these cases are 11 and 10 nm, respectively (the average deviation is $\varepsilon = 0.5$). The parabolic model normally yields a value 3–9% higher; for the indicated cases $a = 12$ and 11 nm, respectively. This analysis led us to conclude that the shape of the DNA–surfactant is a flattened tore.
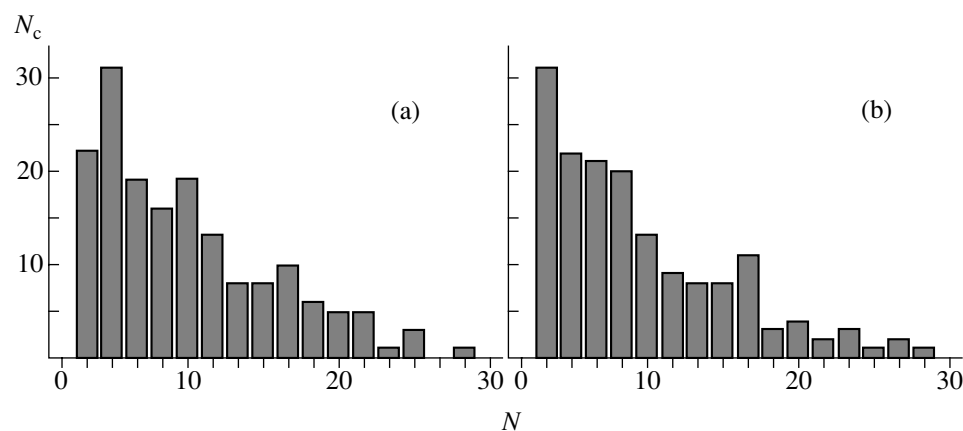
Fig. 5. Histograms of the distribution of DNA–surfactant complexes (N) on the number of DMA molecules in the complex at various radii of curvature of the probing tip R: (a) 6 and (b) 12 nm; N_c is the number of complexes.

We also calculated the number of molecules comprising long filaments in the aqueous phase after the completion of the transfer of DNA–surfactant complexes into the organic phase (see above). Using the FWHM d and the height ($h = 2b$) of the images these structures (0.3–0.9 and 13–25 nm, respectively), we obtained their real dimensions: $a = 5$–11 nm at $R = 6$ nm and $a = 6$–12 nm at $R = 12$ nm. On average, the cross section of a filament contains from 1 to 5 DNA molecules. Thus, the proposed approach yields results that are in agreement with the expected values for both single DNA molecules and their aggregates.

Note that the proposed model does not take into account the contribution to image broadening associated with motions caused by the lateral interaction of the object with the probing needle during scanning. This effect may prove important under the experimental conditions used in this study (measurements in air). Our estimates show that this effect is largely important for objects with a small cross section (for example, single DNA molecules); in this case, the width of the object d (and hence, a) can be overestimated by a factor of 1.5–2.5.

To limit the influence of this effect, it is necessary to weaken the interaction of the probing needle with the object. This can be achieved by using the intermittent contact regime, especially in the case of liquid media [6]. For example, studying single DNA molecules adsorbed at the mica surface in an aqueous-alcohol medium (more than 40% isopropanol), we obtained the following height and FWHM of the AFM image: $h = 2b = 1.4$–1.8 nm and $d = 5$–8 nm. Then we calculated $a = 1.2$–1.8 nm under the assumption of constancy of molecular volume during deformation ($\pi ab = \pi r^2$, where $r = 1$ nm is the model radius of the DNA molecule). In more detail, these results will be published elsewhere.

We assumed that the packing of the DNA molecules is hexagonal; then the molecular volume is given by

$$4r^2 L \sin 60°,$$

where r is the radius of the DNA molecule, and L is its length. The volume of the toroidal complex is given by $\pi^2 abD$, where a is the numerically determined value, $b = h/2$, and D is the tore diameter. Taking into account the presence of a surfactant coating of thickness l, we obtained the formula for the number of molecules:

$$N = \pi^2 abD / 2\sqrt{3}(r + l)^2 L.$$

The histograms of the distribution of complexes over the number of constituent molecules at $R = 6$ nm and $R = 12$ nm are displayed in Fig. 5 (the parabolic model yields practically the same distributions). An analysis of these histograms shows that about 80% of the complexes contain less than 16 DNA molecules (as estimated at $R = 6$ nm) or 15 (at $R = 12$ nm).

REFERENCES

1. Bloomfield, V.A., *Biopolymers*, 1991, vol. 31, p. 1471.
2. Sergeev, V.G., Pyshkina, O.A., Gallyamov, M.O., *et al.*, *Progr. Colloid Polym. Sci.*, 1997, vol. 106, p. 198.
3. Pyshkina, O.A., Sergeev, V.G., Zezin, A.B., and Kabanov, V.A., *Dokl. Ross. Akad. Nauk*, 1996, vol. 348, no. 4, p. 496.
4. Pyshkina, O.A., DNA–Surfactant Complexes in Low-Polarity Organic Solvents, *Cand. Sci. (Chem.) Dissertation*, Moscow: Moscow State Univ., 1997.

5. Binnig, G., Quate, C.F., and Gerber, Ch., *Phys. Rev. Lett.*, 1986, vol. 56, p. 930.

6. *Skaniruyushchaya zondovaya mikroskopiya biopolimerov* (Scanning Probing Microscopy of Biopolymers), Yaminskii, I.V., Ed., Moscow: Nauchnyi Mir, 1997, pp. 25–40.

7. Gallyamov, M.O., Drygin, Yu.F., and Yaminskii, I.V., *Poverkhnost* (in press).

8. Hansma, H.G., Vesenka, J., Siegerist, C., *et al.*, *Science* (Washington, DC), 1992, vol. 256, p. 1180.

9. Sergeev, V.G., Pyshkina, O.A., Zezin, A.B., and Kabanov, V.A., *Vysokomol. Soedin., Ser. A*, 1997, vol. 39, no. 1, p. 17.

10. Murray, M.N., Hansma, H.G., Bezanilla, M., *et al.*, *Proc. Natl. Acad. Sci. USA*, 1993, vol. 90, p. 3811.

11. Garcia, V.J., Martinez, L., Briceno-Valero, J.M., and Schilling, C.H., *Probe Microscopy*, 1998, vol. 1, no. 2, p. 117.

12. Drygin, Yu.F., Bordunova, O.A., Gallyamov, M.O., and Yaminsky, I.V., *FEBS Lett.*, 1998, vol. 425, p. 217.